How to cite: *Angew. Chem. Int. Ed.* **2024**, *63*, e202313947
doi.org/10.1002/anie.202313947

Protein Dynamics

Microsecond Timescale Conformational Dynamics of a Small-Molecule Ligand within the Active Site of a Protein

*Julia Kotschy[#], Benedikt Söldner[#], Himanshu Singh, Suresh K. Vasa, and Rasmus Linser**

Abstract: The possible internal dynamics of non-isotope-labeled small-molecule ligands inside a target protein is inherently difficult to capture. Whereas high crystallographic temperature factors can denote either static disorder or motion, even moieties with very low B-factors can be subject to vivid motion between symmetry-related sites. Here we report the experimental identification of internal µs timescale dynamics of a high-affinity, natural-abundance ligand tightly bound to the enzyme human carbonic anhydrase II (hCAII) even within a crystalline lattice. The rotamer jumps of the ligand's benzene group manifest themselves both, in solution and fast magic-angle spinning solid-state NMR ^{1}H $R_{1\rho}$ relaxation dispersion, for which we obtain further mechanistic insights from molecular-dynamics (MD) simulations. The experimental confirmation of rotameric jumps in bound ligands within proteins in solution or the crystalline state may improve understanding of host-guest interactions in biology and supra-molecular chemistry and may facilitate medicinal chemistry for future drug campaigns.

Protein-ligand complexes are usually explored via crystallographic studies, which in case of structurally rigid ligands can accurately report on the underlying site-specific interactions. Conversely, for structural elements with enthalpically less restricted interactions to the target, X-ray crystallographic electron density maps often indicate heterogeneity and/or flexibility of atoms via increased B-factors.[1] However, motion cannot confidently be distinguished from static disorder with a single complex structure, and in particular exchange between like conformations remains elusive.[2] With cryo-electron microscopy, molecules can be trapped at different points in time to assess larger structural differences (non-equivalent conformations),[3] but timescale information is unavailable. In particular, motion in the µs regime, a hallmark of enzymatic catalysis and recognition at physiological temperatures, which for *proteins* has constituted a prime focus of structural biology, has been difficult to observe for bound *ligands*, including substrates or small-molecule messengers.

Compared to their entropic losses through rigid-body motion of around 15–20 kJ/mol,[4] configurational entropy losses upon binding have been estimated to reach up to 100 kJ/mol.[5] Finetuning of residual ligand mobility in the bound state thus has important consequences for the overall entropic contributions ($-T\Delta S$, normally a few tens of kJ/mol) to the binding affinity.[6] Although in silico predictions have become increasingly reliable,[7] the difficulty of site-specific assessment of residual mobility by experiments has set limitations to the understanding of the dynamic properties of host:guest complexes in supramolecular chemistry and catalysis, of substrate affinity and selectivity in natural and synthetic enzymes, for predicting the thermodynamic properties of pharmacological inhibitors, and for the rational optimization of a diverse range of compounds through targeted synthetic and medicinal chemistry.[1b,6,8] While in solution, a plastic behavior and in particular the possibility of protein breathing is known to facilitate internal motion associated with steric restrictions,[9] it has remained unclear whether such conformational exchange, e.g. aromatic ring flips in tightly bound ligands, is maintained within proteins restrained in a crystal lattice.

Here we show that µs timescale rotameric jumps are experimentally observed for a tightly packed, crystallographically well-defined element of a high-affinity pharmaceutical inhibitor in crystalline hCAII. Using proton $R_{1\rho}$ relaxation dispersion in solution and in micro-crystals, combined with MD simulations, internal µs timescale dynamics of a ligand aromatic ring are revealed both in the expectedly more plastic protein in solution and also within the crystalline enzyme.

We prepared natural-abundance, ^{13}C/^{15}N- and ^{2}H/^{13}C/^{15}N-labeled hCAII (Figure 1A), a ubiquitous 29 kDa enzyme and well-studied, FDA-approved drug target interconverting bicarbonate and carbon dioxide, using procedures similar to those established[11] (see the Supporting Information for details). For crystalline samples of hCAII in complex with *(R)*-N-(3-indol-1-yl-2-methyl-propyl)-4-sulfamoyl-benzamide (denoted "SBR" in the following, according to the PDBeChem ligand dictionary, Figure 1B), a high-affinity binder with a K_D of ≈30 pM,[12] the ligand was either soaked into preformed hCAII crystals or added before crystalliza-

[*] J. Kotschy,[#] B. Söldner,[#] Dr. H. Singh, Dr. S. K. Vasa, Prof. Dr. R. Linser
Department of Chemistry and Chemical Biology, TU Dortmund University
Otto-Hahn-Str. 4a, 44227 Dortmund (Germany)
E-mail: rasmus.linser@tu-dortmund.de

[#] co-first authors

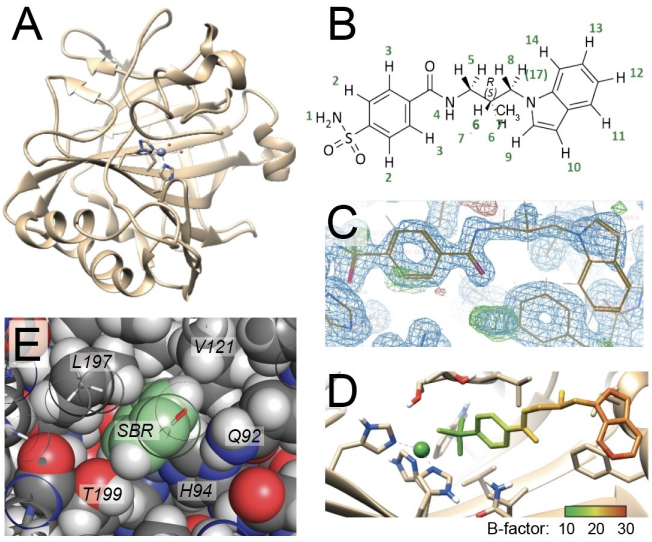

Figure 1. The hCAII-SBR complex. **A**) hCAII crystal structure in apo form (PDB 3gz0).[10] **B**) Ligand SBR, depicting sequential numbering colored in green as used throughout this study. Protons 2 and 3 are called benzylic protons and protons 9–14 indole protons in the following. **C**) Ligand electron densities in X-ray crystallographic data of the co-crystalline sample at cryogenic temperatures, deposited under PDB ID 8R1I. **D**) Representation of ligand B-factors of this sample (color code below). **E**) Packing of the benzene moiety of SBR (green) deep inside the active-site pocket.

tion (co-crystallization). As a reference to NMR-spectroscopic studies, both types of crystals were subjected to X-ray diffraction, the co-crystallized structure with a resolution of 1.46 Å revealing better-defined electron densities for SBR than the soaked sample (see Figures S1 and S2 as well as Tables S1 and S2 in the SI). B-factors within the SBR ligand, which estimate the atomic displacement from its average position, imply strong conformational heterogeneity or flexibility near the indole group (B-factors up to 32 even for the co-crystallized complex). By contrast, the structural elements close to the Zn^{2+}-bound warhead ($\approx$14) and the benzene ($\approx$17) appear highly defined. Figure 1C and D show the electron densities as well as the temperature B-factors, respectively, for the SBR ligand bound to hCAII upon co-crystallization. Figure 1E represents the dense packing of its benzene ring in the pocket.

We wondered whether there is any "hidden" motion of SBR in the hCAII complex crystals for the crystallographically well-defined aromatic ring, similar to observations of aromatic ring flips in amino acid side chains recently identified by ^{13}C relaxation dispersion.[13] First, solution NMR characterization of the complex with a ^{13}C,^{15}N-labeled protein was pursued after concentration of the sample in 50 mM phosphate buffer to $\approx$8.5 mg/ml and titration of an equimolar amount of SBR into the solution. Figures S3 and S4 show the chemical-shift perturbations (CSPs) of hCAII *amide peaks* upon addition of SBR. Regions in which the highest CSPs for backbone spins cluster comprise amino acids 125–142 and 198–205, both close to the binding pocket. In agreement with the X-ray data, the titration data confirm a single binding site of the ligand. Importantly, the data also confirm a residence time longer than the NMR timescale,[14] as expected from the dative bond between warhead and Zn^{2+}, which avoids interference of ligand association/dissociation with the relaxation dispersion studies in the following. To further rule out contributions from potential backbone motion in such data, we performed ^{15}N relaxation dispersion, reporting on (local) shift fluctuations for the amides (Figure S5A). In consistency with previous work employing two other sulfonamide inhibitors,[11,15] the data confirm that any intrinsic µs timescale motion in the pocket of *apo* hCAII is quenched upon binding of the ligand. ^{1}H $R_{1\rho}$ relaxation dispersion experiments of the apo ligand on its own (Figure S5B) do not show dispersion either.

Access to site-specific *ligand resonances* and their properties in the bound state in solution without interference from protein nuclei was obtained by a combination of $^{15}N/^{13}C$-filtered[16] 2D $^{1}H/^{1}H$ correlations (with a relay transfer) with water suppression modules and an $R_{1\rho}$ relaxation block (see Figure S6 for the pulse sequence) on $^{13}C/^{15}N$-labeled hCAII. Peak assignments were transferable from spectra of the apo ligand in D_2O (Figures S7, S8, and S10). We recorded ^{1}H $R_{1\rho}$ relaxation dispersion profiles (Figures 2C and S9) to probe the possible µs timescale conformational-exchange dynamics of the ligand in the active site. To combat proton-proton cross relaxation, ^{1}H $R_{1\rho}$ data were recorded in a constant-time fashion using a spin lock at 35.3°, at which angle NOESY and ROESY contributions cancel.[17] In contrast to the absolute values, which are susceptible to overall tumbling, the existence of Bloch-McConnell relaxation dispersion (BMRD) found for varying spin lock field strengths can report on slow-motional internal contributions (Figure 2A).[18] Figures 2C and Figure S9 show that a dispersive behavior is indeed observed for cross peaks representing the benzylic ring, whereas expectedly, neither of the indole protons shows a clear dispersion profile. Even though the signal-to-noise ratio in the filtered experiments as well as chemical-shift differences for chemically equivalent protons (in the apo state) in different rotameric states (in the complex) and hence dispersion effects are expectedly small, the dispersion curves for part of the peaks meet the statistical criteria ($p < 0.05$) to suggest a flipping motion of the benzylic ring on a tens of µs timescale while bound to hCAII in solution. By contrast, the flat profiles of the indole protons at rather high baseline $R_{1\rho}$ rates (around $7\,s^{-1}$) denote faster motion, exceeding the timescale accessible by the available spin lock field strengths, however, still significantly slower than the dynamics of the free ligand (see apo vs. bound-ligand linewidths in Table S3).

Motion has been reported to be highly similar between proteins in solution and those in a crystalline setting.[19] Still, the lattice might reduce breathing motion and thus abrogate dynamics of tightly packed ligand moieties. To assess whether the apparent conformational exchange of the bound ligand is maintained even in the context of the crystal, we composed a proton-detected $^{13}C/^{15}N$ double-filtered ^{1}H $R_{1\rho}$-edited sequence with tailored water suppression modules for solid-state NMR at fast magic-angle spinning. (See a protein H/N spectrum of micro-crystalline, co-crystallized hCAII/

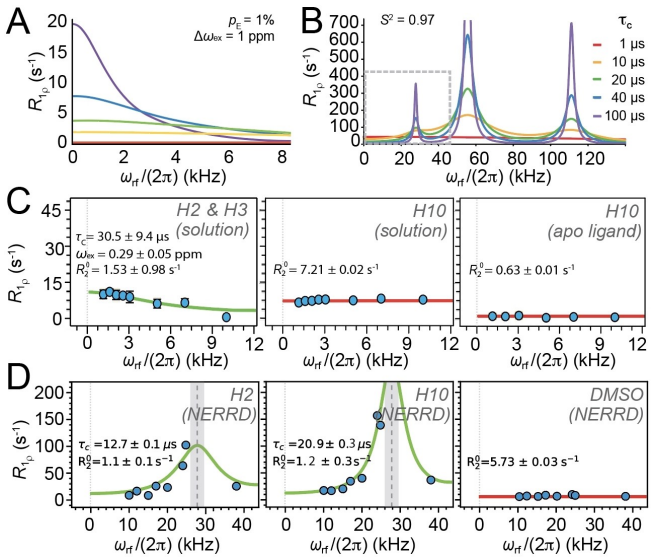

Figure 2. Slow-motional ligand dynamics assessed via ^{1}H ligand relaxation dispersion in solution and in the solid state. **A**) ^{1}H $R_{1\rho}$ BMRD relaxation dispersion curves simulated for populations p_E of 1 % and a chemical-shift difference $\Delta\omega_{ex}$ of 1 ppm for different timescales of exchange. **B**) Simulated profiles of proton NERRD at 55.555 kHz MAS for different time regimes of motion (considering homonuclear interactions with 3 Å effective distance and a CSA of 10 ppm at 700 MHz ^{1}H Larmor frequency at an S^2 of 0.97). The dashed box denotes the regime (around the HORROR condition) investigated here. **C**) Ligand µs timescale motion in the complex, seen only in ^{1}H BMRD profiles of benzylic protons (left), opposed to motion faster than refocussed by the spin lock for indole protons (center) and much faster motion for apo ligand in general (right). See more profiles in Figures S5B and S9. **D**) NERRD behavior observed in the co-crystallized hCAII/SBR sample for all discernable ligand proton signals, including the benzyl and the indole ring (left and center, respectively), but not for residual DMSO as a reference case for isotropic motion outside the µs regime (right). (See more profiles in Figure S14.) Spins are numbered (gray/italic) as shown in Figure 1B. The dashed gray lines in D) denote the HORROR condition at 27.777 kHz. Note that the amplitude of the ^{1}H NERRD profiles depends on the strength of the effective proton-proton dipolar network at the site, which in the presence of motion is a time-dependent property that as of now is hard to predict (see the Supporting Information Text). This blurs an assessment of motional amplitudes and at this point reduces the quantitative assessment to a timescale information.

SBR complex in Figure S11; the ^{1}H $R_{1\rho}$-edited pulse sequence and a filtered spectrum of the ligand only are shown in Figures S12 and S13, respectively). In the solid state, assessing fast-timescale ligand motion is again compromised by the unavailability of NMR-active heteronuclei. Redfield-type auto relaxation of protons as well as assessment of slow conformational exchange by BMRD are limited by strong coherent contributions to the effective rates and small chemical-shift differences between states. However, proton near-rotary resonance relaxation dispersion (^{1}H NERRD), introduced in theory[20] and for two model proteins[21] recently, is responsive to µs-ms timescale changes in the regional homonuclear dipolar networks and hence relative bond orientation, rather than to changes in isotropic chemical shifts. Figure 2B shows a simulation of the ^{1}H NERRD effect for a range of timescales. The measurement benefits from a high amplitude of dispersion for a natural-abundance nucleus in case of µs-timescale architectural changes in the dipolar network close to the half-rotary-resonance (HORROR) condition. On the flip-side, amplitude information is blurred as the effective strength of the interaction cannot be accurately determined.[20,21b]

Peak assignments of hCAII-bound SBR in the solid state were transferred from the complex in solution, tolerating deviations of up to 0.2 ppm due to likely temperature inaccuracies. Owing to partial peak overlap, four signals were assessed that in part entangle multiple protons each, namely 3/11/14 and 12/13, in addition to proton 2 and proton 10. Profiles of the latter two peaks, representatives of one of the aromatic systems each, are depicted in Figure 2D. (See the others, as well as dispersion curves of protein amides from previous work for comparison, in Figure S14.) Note that in contrast to the *local* (chemical-shift) changes probed in BMRD, changes in a tightly coupled proton-proton dipolar network in case of µs timescale contributions for one of the rings would be felt by protons from both rings. (See a more detailed assessment below.) This is reflected in the distinct NERRD profiles, where fast µs timescale contributions, with timescales between 5 and 20 µs, variable amplitudes, and maximal $R_1\rho$ rates up to $\approx$200 s^{-1}, show for both rings. The DMSO solvent peak, by contrast, with an isotropic motion much faster than the µs regime, displays a flat profile of the fast-motional case with constantly low $R_{1\rho}$ rates of around 6 s^{-1} only (bottom-right profile in Figure 2D).

To understand the slow motional components for the ligand mechanistically, we conducted MD simulations on the system in GROMACS with the Amber ff19SB force field. For this purpose, the system was prepared with the AmberTools22 package, including parametrization of the zinc cofactor with the metal center parameter builder.[22] (See details in the SI.) Three production runs for 4 µs each were performed for the SBR-bound form in addition to 2 µs for the apo-form. In contrast to most of the protein backbone, being rather rigid over the course of the simulation (apart from the very N-terminus and residues around sites G234, A133, L84, and P21, see Figure S17 for residue-resolved root mean square fluctuations of the protein in apo and SBR-bound states), the ligand itself again displays a large spectrum of dynamics. Most of these motions are expectedly fast (ns timescale dynamics, see Figures 3A/B and C) outside the sensitivity of NERRD experiments and in line with the flat BMRD profiles for the ligand tail. Intriguingly, by contrast, the benzylic ring, the central element between the sulfonamide warhead and the attached indole moiety, displays $\approx$180° rotameric jumps on the µs timescale, determined by its tight π-interaction with the side chain of Leu197[23] (Figures 3B, red trace, 3D, and S18/19). In consistency, three rotameric jumps, two of them within a short period with a 30° twist relative to the major rotamer, are also observed in the third trajectory (Figure S18E). Both, the intrinsic insufficiencies of the MD force fields as well as insufficient sampling of the event in the 4 µs

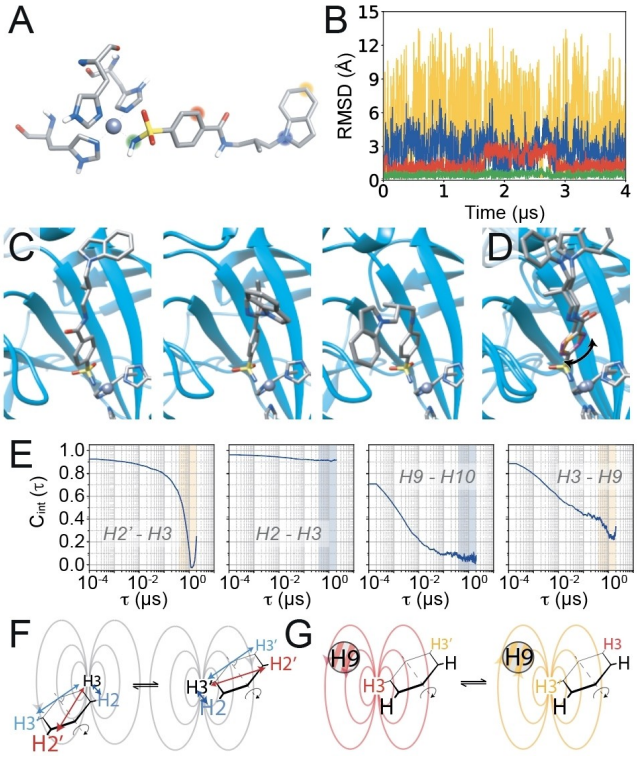

Figure 3. Different modes of ligand dynamics, including aromatic ring flips on the μs timescale, as seen in MD simulations. **A**) Constitution of the ligand within the protein, showing colors employed in B. **B**) Root-mean-square deviations (RMSDs) of individual ligand protons as a function of simulation time, red reflecting the benzylic ring flip on the μs timescale. **C**) Excerpts from a 4 μs trajectory giving representative positions of the fast but non-isotropic motion of the indole ring (three snapshots) and **D**) the ≈180 ° ring flip of the benzylic ring (two snapshots overlayed). For visualization, the ring has different colors on different sides. **E**) Time correlation functions (TCFs, shown up to half the simulation time) of different intra-ring (H2′-H3, left; H2-H3, second from the left; H9-H10, third from the left) and inter-ring vectors (H3-H9, right), the fast μs timescale regime marked in orange (present) or blue (absent). In contrast to the interaction between protons on the same side (e.g., H3 and H2, vector parallel to the rotation axis) and that between the C_2-symmetry-related protons (e.g., H3 and H3′, 180° flip of the inter-spin vector), only the diagonal protons in the benzylic ring (e.g., H3 and H2′) cause a flip-dependent modulation of the local fields. Whereas intra-indole vectors like between H9 and H10 represent purely fast-timescale modulations, *inter*-ring interactions bear fast and slow-timescale contributions modulating the local magnetic fields. **F**) Visualization of the reconstitution of the (*intra*-ring) dipolar network after a ≈180 ° benzene flip (exemplarily shown for H3) both, with regard to the symmetry-related partner (H3′) as well as for the directly adjacent proton (H2) (see text for details). **G**) μs timescale *inter*-ring modulation of the effective dipolar network around an indole proton (top left) due to a benzene flip. Benzene flips further modulate the fast-timescale average of the local magnetic fields in the indole imposed by intra-indole dipolar interactions (and vice versa). A modulation applies whenever interchanging protons 3 and 3′ (or 2 and 2′ or both) have opposite spin state (here visualized by red vs. orange color).

simulations prevent accurate determination of the timescale of the flips. However, qualitatively, their sparsity (five 180° flips in 12 μs in total) is well in agreement with the μs timescale observed experimentally. Both is in congruence with the spectrum of timescales observed for ring flips in aromatic sidechains of protein amino acids.[9a,c,13]

Figure 3E displays three representative time correlation functions (TCFs) for different (intra- and inter-ring) proton-proton internuclear vectors, obtained from the MD trajectory as described by Hoffmann et al.[24] (More TCFs are shown in Figures S20–S22, see the Supporting Information text for more details.) The TCFs represent time-dependent changes of the individual contributions to the local magnetic field at a given site, i.e., the fluctuating dipolar interaction strength dependent on relative movement of one proton to the other, equally affecting both protons. Due to the point symmetry of the nuclear magnetic field, after a 180° ring flip, two out of three (intra-ring) dipolar interactions for the benzylic protons impose local magnetic fields of the exact same magnitude and direction as before the flip (blue coupling partners in Figure 3F; second TCF in Figure 3E). Only one proton in the ring (red, with a ≈5 Å distance) causes changes to the local magnetic field (first TCF in Figure 3E). The fast-timescale dynamics of the indole moiety average the *intra*-indole dipolar interactions on a timescale inaccessible for NERRD (third TCF in Figure 3E). However, the benzylic ring flips further modulate the fast-timescale average of the local magnetic field at the indole protons by additional *inter*-ring interactions (fourth TCF in Figure 3E) on the μs timescale. This is the case when α spins in the benzyl ring (e.g., H2 or H3) interconvert with β spins (when H2′ or H3′, respectively, have opposite spin state) and vice versa, i.e., in 50 % of the cases (Figure 3G). By contrast, for exchange between like spin states in the benzyl ring, the effective inter-ring dipolar network is reconstituted. Given the high plasticity of the overall ligand structure (Figure 3C), the effective distances applicable for inter-ring modulations of the local magnetic fields vary strongly (see Figure S23). As such, the inter-ring proton-proton distances do reach below 5 Å, which distance also determines the *intra*-benzylic (H3/H2′) contribution. The experimental NERRD profiles are hence reconcilable with the mechanistic assessment by MD.

While each of the above assessments has its technical limitations, in conjunction, the above data for the SBR ligand strongly prompt that moieties with highly defined electron densities can comprise hard-to-detect μs timescale conformational exchange motion even in the crystalline state. In structure-based drug design and medicinal chemistry, the understanding of internal dynamics for high-affinity ligands on different timescales has been limited, and its demonstration for hCAII and a sulfonamide ligand, a prototypical pair of protein and inhibitor, via NMR may open several new avenues. The quantitative information content conveyed by the individual experiments exploiting natural-abundance proton relaxation dispersion is limited by several factors mentioned along the above findings. Nevertheless, even qualitative *identification* of ligand dynamics, its temperature dependence, or its abrogation by mutations or upon changes of external conditions, may help better understand host-guest interactions. This has the mentioned consequences for the evaluation and optimization of affinity and entropy in synthetic small-molecule ligands, e.g. phar-

macological binders, for supramolecular chemistry and structural biology of protein-ligand complexes but equally concerns natural or biotechnological processes (inhibitors, substrates, or products), as well as studies involving nucleotides or small DNA or RNA molecules, which pose similar limitations to isotope labelling. We expect that in particular for solid samples, with new prospects for NMR-restrained MD simulations,[25] higher magnetic fields, and increasing MAS rates,[26] an exploitation of ^{1}H relaxation dispersion will bring a greenfield of hitherto inaccessible applications.

In conclusion, we have demonstrated the experimental detection of fast µs timescale dynamics in a sterically restrained part of a high-affinity ligand while bound to its target protein, even in the context of the crystal lattice. Although a quantitative level as known for heteronuclear relaxation is yet unavailable for ^{1}H relaxation dispersion due to the difficulty of quantifying the interaction strength, the obtained profiles for the first time identify and distinguish motion on the µs timescale for a non-isotopically labeled target compound in solution and in the crystalline state, which brings about new perspectives for understanding and tailoring host-guest chemistry.

Chemical-shift assignments and X-ray data were deposited into the BMRB (ID 52196) and the PDB (ID 8R1I), respectively.

Acknowledgements

We are grateful for the SBR ligand, synthesized by Hans-Dieter Gerber and Prof Gerhard Klebe, Marburg University, critical reading of the manuscript by Prof Lars Schäfer (Ruhr Uni Bochum), continuous inspiration from Dr Tomas Jacso (Amgen Research) on the topic, and for big support with X-ray data by Dr. Raphael Gasper (MPI Dortmund). Funded by the Deutsche Forschungsgemeinschaft (DFG, German Research Foundation) under Germany's Excellence Strategy—EXC 2033—390677874—RESOLV, and EXC-114—24286268—CiPS-M. Funded by the Deutsche Forschungsgemeinschaft (DFG, German Research Foundation)—27112786, 325871075, the Emmy Noether program (to R.L.), and a Kekulé Fellowship from the Fonds der Chemischen Industrie (to J.K.). Open Access funding enabled and organized by Projekt DEAL.

Conflict of Interest

The authors declare no conflict of interest.

Data Availability Statement

The data that support the findings of this study are openly available in the BMRB at bmrb.wisc.edu/, reference number 52196, and in the PDB at https://www.rcsb.org, reference number 8R1I.

Keywords: Ligand Entropy · Protein Complexes · Protein Dynamics · Proton Detection · Solid-State NMR

[1] a) D. Ringe, G. A. Petsko, *Methods Enzymol.* **1986**, *131*, 389–433; b) C. Gerlach, M. Smolinski, H. Steuber, C. A. Sotriffer, A. Heine, D. G. Hangauer, G. Klebe, *Angew. Chem. Int. Ed.* **2007**, *46*, 8511–8514.
[2] G. E. Bacon, N. A. Curry, S. A. Wilson, R. Spence, *Proc. R. Soc. London Ser. A* **1997**, *279*, 98–110.
[3] N. Fischer, A. L. Konevega, W. Wintermeyer, M. V. Rodnina, H. Stark, *Nature* **2010**, *466*, 329–333.
[4] a) C. W. Murray, M. L. Verdonk, *J. Comput.-Aided Mol. Des.* **2002**, *16*, 741–753; b) M. Nazaré, H. Matter, D. W. Will, M. Wagner, M. Urmann, J. Czech, H. Schreuder, A. Bauer, K. Ritter, V. Wehner, *Angew. Chem. Int. Ed.* **2012**, *51*, 905–911.
[5] C. E. Chang, W. Chen, M. K. Gilson, *Proc. Natl. Acad. Sci. USA* **2007**, *104*, 1534–1539.
[6] G. Klebe, *Nat. Rev. Drug Discovery* **2015**, *14*, 95–110.
[7] L. Chan, G. M. Morris, G. R. Hutchison, *J. Chem. Theory Comput.* **2021**, *17*, 2099–2106.
[8] V. M. Krishnamurthy, B. R. Bohall, V. Semetey, G. M. Whitesides, *J. Am. Chem. Soc.* **2006**, *128*, 5802–5812.
[9] a) L. Mariño Pérez, F. S. Ielasi, L. M. Bessa, D. Maurin, J. Kragelj, M. Blackledge, N. Salvi, G. Bouvignies, A. Palencia, M. Ringkjøbing Jensen, *Nature* **2022**, *602*, 695–700; b) K. Wüthrich, G. Wagner, *FEBS Lett.* **1975**, *50*, 265–268; c) M. Akke, U. Weininger, *J. Phys. Chem. B* **2023**, *127*, 591–599.
[10] B. S. Avvaru, S. A. Busby, M. J. Chalmers, P. R. Griffin, B. Venkatakrishnan, M. Agbandje-McKenna, D. N. Silverman, R. McKenna, *Biochemistry* **2009**, *48*, 7365–7372.
[11] a) S. K. Vasa, H. Singh, P. Rovó, R. Linser, *J. Phys. Chem. Lett.* **2018**, *9*, 1307–1311; b) S. K. Vasa, H. Singh, K. Grohe, R. Linser, *Angew. Chem. Int. Ed.* **2019**, *58*, 5758–5762.
[12] B. A. Grzybowski, A. V. Ishchenko, C. Y. Kim, G. Topalov, R. Chapman, D. W. Christianson, G. M. Whitesides, E. I. Shakhnovich, *Proc. Natl. Acad. Sci. USA* **2002**, *99*, 1270–1273.
[13] a) D. F. Gauto, O. O. Lebedenko, L. M. Becker, I. Ayala, R. Lichtenecker, N. R. Skrynnikov, P. Schanda, *J. Struct. Biol.* **2023**, *7*, 100079; b) D. F. Gauto, P. Macek, A. Barducci, H. Fraga, A. Hessel, T. Terauchi, D. Gajan, Y. Miyanoiri, J. Boisbouvier, R. Lichtenecker, M. Kainosho, P. Schanda, *J. Am. Chem. Soc.* **2019**, *141*, 11183–11195.
[14] A. D. Gossert, W. Jahnke, *Prog. Nucl. Magn. Reson. Spectrosc.* **2016**, *97*, 82–125.
[15] a) H. Singh, C. K. Das, S. K. Vasa, K. Grohe, L. V. Schäfer, R. Linser, *Angew. Chem. Int. Ed.* **2020**, *59*, 22916–22921; b) H. Singh, S. K. Vasa, H. Jangra, P. Rovó, C. Päslack, C. K. Das, H. Zipse, L. V. Schäfer, R. Linser, *J. Am. Chem. Soc.* **2019**, *141*, 19276–19288.
[16] A. L. Breeze, *Prog. Nucl. Magn. Reson. Spectrosc.* **2000**, *36*, 323–372.
[17] T.-L. Hwang, S. Mori, A. J. Shaka, P. C. M. van Zijl, *J. Am. Chem. Soc.* **1997**, *119*, 6203–6204.
[18] A. G. Palmer, *Chem. Rev.* **2004**, *104*, 3623–3640.
[19] a) V. Chevelkov, Y. Xue, R. Linser, N. Skrynnikov, B. Reif, *J. Am. Chem. Soc.* **2010**, *132*, 5015–5017; b) P. Schanda, M. Ernst, *Prog. Nucl. Magn. Reson. Spectrosc.* **2016**, *96*, 1–46.
[20] P. Rovó, R. Linser, *J. Phys. Chem. B* **2017**, *121*, 6117–6130.
[21] a) D. F. Gauto, A. Hessel, P. Rovó, V. Kurauskas, R. Linser, P. Schanda, *Solid State Nucl. Magn. Reson.* **2017**, *87*, 86–95; b) P. Rovó, C. A. Smith, D. Gauto, B. L. de Groot, P. Schanda, R. Linser, *J. Am. Chem. Soc.* **2019**, *141*, 858–869.
[22] P. Li, K. M. Merz, *J. Chem. Inf. Model.* **2016**, *56*, 599–604.
[23] S. Glöckner, K. Ngo, C. P. Sager, T. Hüfner-Wulsdorf, A. Heine, G. Klebe, *ACS Chem. Biol.* **2020**, *15*, 675–685.

[24] F. Hoffmann, F. A. A. Mulder, L. V. Schäfer, *J. Chem. Phys.* **2020**, *152*, 084102.
[25] B. Söldner, K. Grohe, P. Neidig, J. Auch, S. Blach, A. Klein, S. K. Vasa, L. V. Schäfer, R. Linser, *J. Phys. Chem. Lett.* **2023**, *14*, 1725–1731.
[26] a) M. Callon, D. Luder, A. A. Malär, T. Wiegand, V. Římal, L. Lecoq, A. Böckmann, A. Samoson, B. H. Meier, *Chem. Sci.* **2023**, *14*, 10824–10834; b) T. Le Marchand, T. Schubeis, M. Bonaccorsi, P. Paluch, D. Lalli, A. J. Pell, L. B. Andreas, K. Jaudzems, J. Stanek, G. Pintacuda, *Chem. Rev.* **2022**, *122*, 9943–10018.

Manuscript received: September 18, 2023
Accepted manuscript online: November 16, 2023
Version of record online: December 15, 2023